# Transient dynamics of soft particle glasses in startup shear flow. Part II: Memory and aging

Bruno Flavio Di Dio; Fardin Khabaz; Roger T. Bonnecaze; ... et. al



Journal of Rheology 66, 717–730 (2022) https://doi.org/10.1122/8.0000448





CrossMark

#### **Related Content**

Capillary pressure determination an Iraqi carbonate reservoir-Shuaiba reservoir/Khabaz field/North of Iraq AIP Conference Proceedings (July 2022)

Transient dynamics of soft particle glasses in startup shear flow. Part I: Microstructure and time scales

Journal of Rheology (March 2021)

Predicting permeability by integrating FZI approach with rock typing in heterogeneous carbonate reservoir

AIP Conference Proceedings (July 2022)



# Transient dynamics of soft particle glasses in startup shear flow. Part II: Memory and aging

Bruno Flavio Di Dio, <sup>1</sup> Fardin Khabaz, <sup>2,3</sup> Roger T. Bonnecaze, <sup>4</sup> and Michel Cloitre <sup>1,a)</sup>

<sup>1</sup>Molecular, Macromolecular Chemistry, and Materials, ESPCI Paris, CNRS, PSL University, 10 Rue Vauquelin, 75005 Paris, France

<sup>2</sup>School of Polymer Science and Polymer Engineering, The University of Akron, Akron, Ohio 78712 <sup>3</sup>Department of Chemical, Biomolecular, and Corrosion Engineering, The University of Akron, Akron, Ohio 78712 <sup>4</sup>McKetta Department of Chemical Engineering, The University of Texas at Austin, Austin, Texas 78712

(Received 27 January 2022; final revision received 5 May 2022; published 3 June 2022)

#### **Abstract**

We explore the rheology during a startup flow of well-characterized polyelectrolyte microgel suspensions, which form soft glasses above the jamming concentration. We present and discuss results measured using different mechanical histories focusing on the variations of the static yield stress and yield strain. The behavior of the shear stress growth function is affected by long-lived residual stresses and strains that imprint a slowly decaying mechanical memory inside the materials. The startup flow response is not reversible upon flow reversal and the amplitude of the static yield stress increases with the time elapsed after rejuvenation. We propose an experimental protocol that minimizes the directional memory and we analyze the effect of aging. The static yield strain  $\gamma_p$  and the reduced static yield stress  $\sigma_p/\sigma_y$ , where  $\sigma_y$  is the dynamic yield stress measured from steady flow measurements, are in good agreement with our previous simulations [Khabaz *et al.*, "Transient dynamics of soft particle glasses in a startup shear flow. Part I: Microstructure and time scales," J. Rheol. **65**, 241 (2021)]. Our results demonstrate the need to consider memory and aging effects in transient measurements on soft particle glasses. © 2022 The Society of Rheology. https://doi.org/10.1122/8.0000448

#### I. INTRODUCTION

Soft particle glasses (SPGs) are amorphous materials made of deformable particles that are packed at large volume fractions above the jamming transition [1,2]. Important examples include concentrated emulsions [1], microgel suspensions [3], and concentrated dispersions of hairy particles such as star polymers [4,5] or grafted nanoparticles [6]. In SPGs, each particle is constrained in a cage by elastic repulsive forces and cannot move over long distances unless a mechanical action exceeding the yield point is applied. The macroscopic consequence is that SPGs behave like amorphous solids at rest, which respond elastically to small deformations, whereas they can deform irreversibly and flow under large deformations. Steady shear flow of SPGs is often described using the generic Herschel-Bulkley equation, which relates the shear stress  $\sigma$  to the shear rate  $\dot{\gamma}$  through  $\sigma = \sigma_v + k\dot{\gamma}^n$  where  $\sigma_v$  is the yield stress, k is the consistency parameter, and n is the shear-thinning exponent. Understanding the microscopic mechanisms at the origin of the flow of soft glassy materials has stimulated intense experimental and theoretical research [7,8]. Extensions of mode coupling theory [9], micromechanical models [10,11], and mesoscopic [12-14] and microscopic models [15,16] constitute important contributions to the field. It has been shown that the steady shear and oscillatory rheology of model SPGs

Beyond steady shear rheology, the transient response of SPGs during a startup flow provides important information about the time-dependent mechanisms that drive the solidliquid transition from jammed to fluid states. Startup experiments are performed by applying a constant shear rate at time zero to the material initially kept at rest and analyzing the shear stress growth function that will also be called the transient stress in the following. Experimentally, SPGs made of thermosensitive core–shell particles [9,20,21], polyethylene oxide-protected silica particles [22], multiarm star polymers. [20,23,24], concentrated emulsions [25,26], dispersions of wax crystal in oil [27], and Carbopol suspensions [28,29] % have been found to share a generic phenomenology. Initially, the stress grows linearly with the accumulated strain, which represents the elastic response of the material. At larger strains, the stress keeps on growing and eventually reaches a maximum before decreasing to a steady-state value. The stress overshoot  $(\sigma_n)$  represents the minimum stress that the material has to overcome to start flowing from rest; it is often called the static yield stress. Similarly, the position of the overshoot is called the static yield strain  $(\gamma_p)$ . Both quantities depend on the applied shear rate and several material parameters.

Understanding the way soft glasses yield upon flow inception is an important issue. The control of the startup flow response of soft materials is crucial in many manufacturing processes where pressure overshoots can damage the processing tools or be detrimental to the quality of the final products [30]. On a fundamental level, the transient response of soft

© 2022 by The Society of Rheology, Inc. J. Rheol. 66(4), 717–730 July/August (2022)

is dominated by the elastic contact interactions and the lubrication forces acting between the particles [10,11,17–19].

a) Author to whom correspondence should be addressed; electronic mail: michel.cloitre@espci.psl.eu

materials contains the intimate physical mechanisms at the origin of their complex rheology. A recent statistical physics approach makes a connection between the yield behavior of thermally annealed amorphous materials and the physics of phase transition [31]. Yielding is shown to be either discontinuous akin to a first-order phase transition, corresponding to brittle behavior, or smooth and continuous, i.e., ductile, depending on the degree of annealing of the initial state. Another theoretical framework inspired from the fluidity model associates the presence of stress overshoots to the nucleation and growth of shear bands near the moving walls as a result of nonlocal effects [32]. Stress overshoots are then predicted to vary with the applied shear rate as power laws, which exhibit two distinct exponents in the limit of low and high shear rates. Other theoretical approaches based on shear-transformation-zone theory [33], mode coupling theory [34], molecular dynamic simulations [35,36], and micromechanical models [37,38] attribute a key role to nonaffine deformations that develop in amorphous materials during startup flow.

Recently, we have explored startup flows of SPGs using large-scale three-dimensional particle dynamics simulations at different particle volume fractions and shear rates and proposed the following microscopic mechanisms [38]. The buildup of the stress is driven by an interplay between structural anisotropy due to an accumulation of particles along the compression axis and a depletion along the extension axis combined with extra compression of particles that are soft and deformable. At low shear rates, the stress increase is monotonic and without any stress overshoot. The time scale at which structural anisotropy and the stress are maximum is, thus, correlated to the nonaffine dynamics of SPGs. This mechanism, where structural anisotropy is central, echoes to the previous analysis of flow inception in hard sphere glasses [35] and metallic glasses [37].

In view of the current state of the art, a systematic experimental investigation of flow inception in SPGs is timely and desirable in order to confront theoretical models to real properties. This is the purpose of the present work. We use suspensions of soft and deformable microgels made of crosslinked polyelectrolyte networks, which undergo a jamming transition at high enough concentration where they can be assimilated to disordered packings of athermal frictionless particles, which are in contact as in SPGs [3]. By investigating the startup flow properties of the jammed suspensions, systematically varying the microgel concentration and the suspending fluid viscosity, we have discovered that other parameters of interest concern the mechanical history of the SPGs. Indeed SPGs have the capacity to store longlived residual stresses and strains and to slowly evolve during time [39–41]. Therefore, startup flow experiments may probe materials that are in an unspecified state depending on their mechanical history. It is likely that several data available in the literature are affected by significant uncertainties due to uncontrolled mechanical preparation [38]. First, we show that unlike in our model simulations [38] where the suspensions are mechanically equilibrated before flow inception, startup flow experiments in microgel suspensions are significantly affected by mechanical rejuvenation and subsequent relaxation or recovery of residual stress and strain trapped in the materials during their preparation. Second, we present and discuss the results of startup flow experiments measured for different mechanical histories. For each condition, we analyze the values of the static yield stress  $\sigma_p$  and static yield strain  $\gamma_p$  when the shear rate and the microgel concentration are varied over a wide range of values. We discuss our findings in light of the simulation predictions reported in [38] and recent models from the literature.

The article is organized as follows. In Sec. II, we describe the preparation of microgel suspensions, experimental methods, and some basic rheological characterizations at steady state. Section III is devoted to the results of startup flow experiments themselves and their physical interpretation: effects of mechanical history (Sec. III A) including slow relaxation, memory and reversibility of response, aging (Sec. III B), the effect of shear rate (Sec. III C), and finally, the variations of the static yield stress and static yield strain (Sec. III D). Conclusions and perspectives are presented in Sec. IV.

#### II. MATERIALS AND METHODS

#### A. Sample preparation

We use jammed suspensions of polyelectrolyte microgels provided by Coatex SAS [42]. They are synthesized by semibatch emulsion polymerization at low pH ( $\sim$ 2) in starved conditions from ethyl acrylate (64.5 wt. %), methacrylic acid (34.5 wt. %), and the difunctional crosslinker diallyl phthalate (1 wt. %). Initiators and reactants are fed in a continuous way, the feeding rate and temperature being optimized to  $\frac{5}{6}$ ensure that the conversion rate is constant, and the particle size grows linearly with time. These conditions are known to  $\frac{\delta}{k}$ reduce inhomogeneity of composition and limit the occurrence of dangling chains [3]. At the end of the synthesis, a \( \overline{2} \) stock solution of solid polymer particles in water is obtained. The solid content of the stock solution is determined by thermogravimetry. The radius of gyration  $(R_g)$  and the hydrodynamic radius  $(R_h)$  of the particles are determined by static and dynamic light scattering:  $R_g = 27 \text{ nm}$  and  $R_h = 36 \text{ nm}$ ,  $\frac{\pi}{8}$ respectively. The ratio  $R_g/R_h \cong 0.75$  is of the order of the value expected hard-spheres (0.775).

Microgel suspensions are prepared by diluting the stock solution with ultrapure water and adding sodium hydroxide that ionizes the methacrylic acid units and provokes the swelling of the particles [43]. To facilitate homogenization, we mix two equal volumes of polymer and sodium hydroxide in water. The concentration of the sodium hydroxide solution is exactly adjusted to ionize all the carboxylic functions borne by the microgels. In some samples, water is replaced by a mixture of ultrapure water and glycerol in order to increase the viscosity of the suspending medium ( $\eta_s = 11.5$ and 60 mPa s, respectively). The presence of glycerol does not significantly affect the ionization reaction and suspension properties. Samples are gently stirred to avoid bubbles and kept at rest for at least 48 h before use. In the low concentration limit, swollen microgels have a radius of  $165 \pm 3$  nm with a polydispersity index of about 0.1. At finite concentrations, swelling is regulated by a balance between the osmotic

pressures of ions inside and outside the microgels. Most of the counterions associated with the carboxylate groups are trapped inside the microgels, but a small fraction is free to escape in the solution causing a decrease in the net osmotic pressure responsible for swelling and the shrinking of the microgels [3,44,45]. At higher concentrations, steric deswelling takes over when the particles are densely packed and there is not enough water available to achieve swelling equilibrium [3]. Osmotic deswelling is particularly important for ionic microgels due to the translational entropy of the counterions [42], but it also exists in neutral microgels [46]. An important consequence is that the volume fraction of the microgels is not known accurately, and in the following, we use the polymer concentration (C) expressed in mg  $g^{-1}$  as the control variable.

#### B. Rheological measurements

Rheological measurements are carried out with an Anton Paar MCR 502 rheometer equipped with a cone and plate geometry (50 mm diameter,  $2^{\circ}$  angle, and truncation of 48  $\mu$ m). It is a stress-controlled rheometer that has a controller that allows strain-controlled experiments. The shearing surfaces exhibit a roughness of about 5  $\mu$ m in order to prevent wall slip [47]. To minimize solvent evaporation, the geometry is protected from the exterior by a solvent trap commercially available from Anton Paar (#107716). The atmosphere of the trap is saturated using a small quantity of water. The bottom plate is connected to a Peltier system that controls the temperature at  $20.0 \pm 0.1$  °C. The geometry and the drive system are corrected for inertia and residual torques according to the protocol recommended by the manufacturer.

#### 1. Linear viscoelasticity measurements

Small amplitude shear rheology measurements are performed to probe the viscoelastic properties of the suspensions in the linear response domain. The angular frequency is varied between  $10^{-2}$  and  $10^2$  rad s<sup>-1</sup>, and the strain amplitude is being kept constant to a value of  $\gamma_0 = 5 \times 10^{-3}$ .

#### 2. Flow curve measurements

To measure the flow curves, we apply a logarithmic ramp of shear rates with a sampling resolution of six points per decade, which decreases from  $5 \times 10^2$  to  $10^{-2}$  s<sup>-1</sup>, and for each shear rate value, we record the stress at steady state. At low shear rates, mechanical equilibration is very slow and the ramp measurement results are complemented by the long time stress values deduced from startup flow measurements.

#### 3. Startup flow experiments

Startup flow experiments are performed by applying a constant shear rate to a material initially maintained at rest and monitoring the transient stress response. The shear stress is plotted as a function of the time elapsed since the application of the shear rate or equivalently the actual strain experienced by the material. In these experiments, it is critical to control the response time of the rheometer during transient measurements and check that they do not affect the response from the material itself. In practice, the rheometer is controlled by the FM4.92 firmware that

has been especially optimized by Anton Paar for our transient measurements during flow cessation and startup flow experiments. We have carefully determined response times in real configurations, i.e., when the geometry is loaded with microgel suspensions. The detailed results are presented in the supplementary material [48]. In flow cessation experiments, the response time is of the order of 20 ms in the controlled stress mode and 40 ms in the controlled rate mode (Fig. S1 [48]). In startup flow experiments, the response time required to reach the nominal shear rate is of the order of 30 ms (Fig. S2 [48]). Another limitation is the fastest sampling time acceptable for a decent signal to noise ratio, which is of the order of 10 ms. These conditions restrict the range of accessible shear rates since the stress peak that marks the onset of yielding is not correctly resolved at high shear rates above  $\dot{\gamma} \cong 4 \, \mathrm{s}^{-1}$ .

### C. Rheological characterization of microgel suspensions

#### 1. Determination of the glass transition concentration

Linear viscoelasticity and nonlinear flow properties are used to identify the different states that are encountered when \( \gamma \) the concentration is increased. We follow the procedure already described for similar polyelectrolyte microgels in [3] and later generalized to thermosensitive microgels in [46]. Figure 1(A) shows the variations of the storage modulus  $G' \in \mathbb{R}^{n}$ and loss modulus G'' when the polymer concentration is  $\frac{h}{2}$ increased. At low polymer concentration, the viscoelastic moduli reach terminal relaxation, i.e.,  $G'(\omega)-\omega^2$  and  $G''(\omega)-\omega$  at low frequency, indicating liquidlike behavior. Above  $C = 52.5 \text{ mg g}^{-1}$ , terminal relaxation is no longer  $\frac{\overline{0}}{0}$ accessible and the microgel suspensions behave like viscoelastic solids over the entire frequency range with a nearly frequency-independent storage modulus  $G'(\omega)$  and a much  $\frac{3}{2}$ lower loss modulus  $G''(\omega)$ , which exhibits a minimum  $\mathbb{R}$ around a frequency  $\omega_m$  (see also supplementary material § [48]). Figure 1(B) shows the shear rate dependence of the viscosity of microgel suspensions at increasing concentrations. At low concentration, the viscosity curves have the characteristic shape expected for viscous suspensions: a g Newtonian plateau at low shear rates, shear-thinning behavior at intermediate shear rates, and a second plateau at high shear rates. The low-shear viscosity,  $\eta_0$ , increases by several orders of magnitude when the concentration increases from 0 to  $50 \text{ mg g}^{-1}$ . Above  $C = 52.5 \text{ mg g}^{-1}$ , the Newtonian plateau no longer exists in the shear rate window investigated, indicating that the longest relaxation time exceeds the observation time. Based on the results shown in Fig. 1, we associate the concentration  $C_G = 52.5 \,\mathrm{mg \, g^{-1}}$  with the glass transition concentration above which the suspension behaves like athermal glass with solidlike properties. In this regime, the elasticity is of entropic origin [3].

#### 2. Determination of the soft jamming concentration

We define the plateau modulus  $G_0$  as the value of the storage modulus at angular frequency  $\omega_m$  at which the loss modulus has a shallow minimum. The variations of  $G_0$  with the concentration are plotted in Fig. 2. In the entropic glass

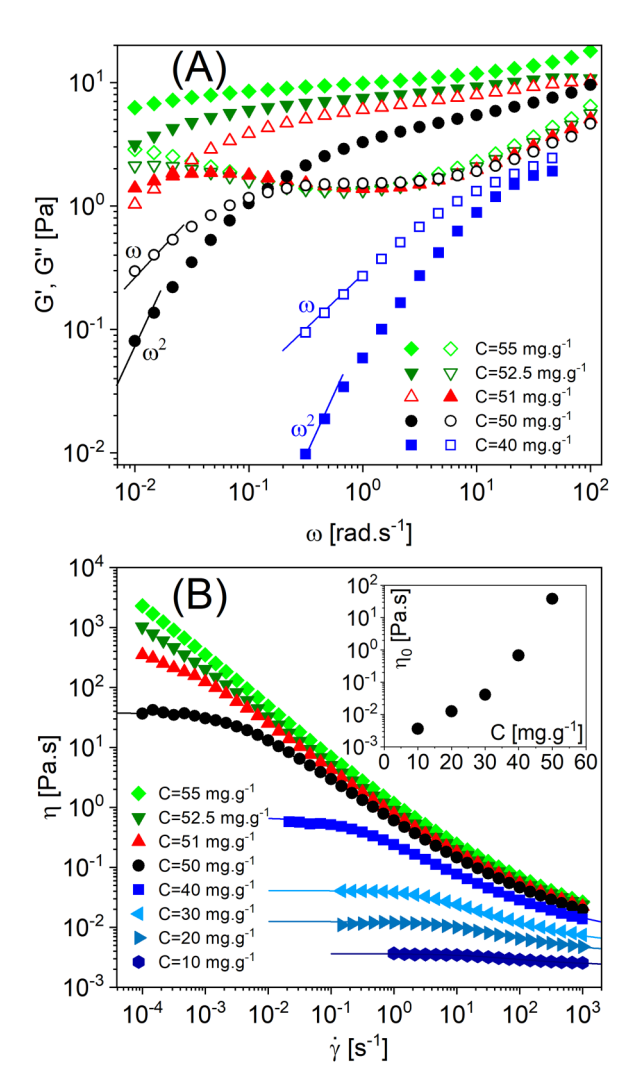


FIG. 1. Viscoelastic moduli vs angular frequency (A) and steady shear viscosity vs shear rate (B) of microgel suspensions with increasing concentration. The inset in (B) shows the variations of the low-shear viscosity with concentration. The continuous lines in (B) are the best fits of the data to the Carreau-Yasuda equation [3].

regime above  $C_G$ , the plateau modulus first increases by several orders of magnitude over a very narrow range of concentration. Similar behavior has already been reported for Brownian hard sphere suspensions [21,49], microgel suspensions of submicron size [3,46], and nanoemulsions [50]. At higher concentration, there is a crossover above which the plateau modulus increases linearly with the polymer concentration. We determine the crossover concentration from the extrapolation to zero modulus of the linear fit to the experimental data. We define this crossover as the onset of the soft jamming regime:  $C_J \cong 10 \text{ mg g}^{-1}$ . In the soft jamming regime, microgel suspensions can be viewed as disordered packings of athermal frictionless particles interacting via repulsive elastic forces that exert through soft and deformable contacts [8,43]. Jamming in microgel suspensions and in other soft particle systems is fundamentally different from jamming in hard sphere suspensions because of the capacity of the particles to be in contact and deform elastically. The linear variation of the plateau modulus agrees with results of simulations for athermal elastic spheres [11,51] and a recent statistical mechanics theory [46].

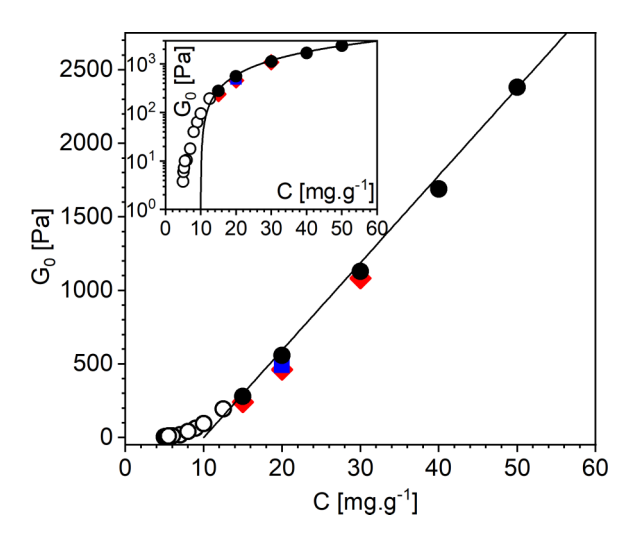


FIG. 2. Variations of the plateau modulus of microgel suspensions as a function of polymer concentration. The suspensions are prepared using pure water (open circle, filled circle:  $\eta_{\rm S}=0.89~{\rm mPa\,s})$  and two water-glycerol mixtures (red filled diamond:  $\eta_{\rm S}=11.5~{\rm mPa\,s}$ ; blue filled square:  $\eta_{\rm S}=60~{\rm mPa\,s}$ ). Open symbols refer to suspensions in the entropic glass regime; full symbols refer to suspensions in the soft jamming regime. The continuous line is the best fit of the data measured in the soft jamming regime to a linear variation. The inset shows the data of the main graph plotted in lin-log representation.

#### 3. Steady flow properties in the soft jamming regime

In the following, we study microgel suspensions at concentrations  $C > C_I$ , i.e., in the soft jamming regime. We vary the  $\frac{\overline{b}}{2}$ polymer concentration and the viscosity of the suspending fluid as shown in Table I. The flow curves  $\sigma(\dot{\gamma})$  are reported in § the supplementary material [48]. They are well fitted to the Herschel-Bulkley equation,  $\sigma = \sigma_v + k\dot{\gamma}^n$  allowing to determine the yield stress  $\sigma_{v}$ , the consistency parameter k, and the shear-thinning exponent n. These parameters are listed in  $\mathbb{R}^2$ Table I. This equation, which has been considered as an empirical form for a long time, has recently emerged from various predictive microscopic theories of soft glasses [10,16,46,52]. Experimentally, the stress amplitude varies linearly with the applied strain up to the yield point allowing us to define the '9 yield strain  $\gamma_v$  as  $\sigma_v = G_0 \gamma_v$  [3,46]. The values of the yield strain are listed in Table I; they are approximately constant indicating that the yield stress and the plateau modulus can be considered as proportional. Following our previous works [1,11,19,53], we scale the stress by the yield stress  $\sigma_v$  and the shear rate by the characteristic time  $\eta_s/G_0$ , which is a particle relaxation time that arises from the balance between viscous and elastic forces. The dimensionless shear rate  $\dot{\gamma}\eta_S/G_0$ expresses the competition between shear advection and particle rearrangement [1,11,19,53]. This set of nondimensional variables collapses all the flow curves on a unique master curve of equation as shown in Fig. 3.

#### III. RESULTS AND DISCUSSION

#### A. Mechanical history

#### 1. Slow relaxation and memory

The rheological study of microgel suspensions, like many other viscoplastic materials, poses specific challenges because of their capacity to accumulate residual stresses and

 $C (\text{mg g}^{-1})$  $\eta_s$  (Pa s)  $G_0$  (Pa) k (Pas<sup>n</sup>) N  $\sigma_{v}$  (Pa)  $\gamma_y(-)$ 15 0.89 280  $13.3 \pm 0.5$  $0.047 \pm 0.02$  $5.4 \pm 0.3$  $0.43 \pm 0.02$ 15 11.5 241  $12.0 \pm 0.5$  $0.050 \pm 0.02$  $11.4 \pm 0.3$  $0.52 \pm 0.02$ 20 565  $0.050 \pm 0.02$  $11.9 \pm 0.2$  $0.39 \pm 0.02$ 0.89  $33 \pm 1$  $0.054 \pm 0.02$ 20 11.5 460  $25 \pm 1$  $21 \pm 1$  $0.48 \pm 0.02$ 20 60 480  $0.051 \pm 0.02$  $40 \pm 1$  $0.50 \pm 0.02$  $25 \pm 1$ 30 0.89 1030  $60 \pm 1$  $0.055 \pm 0.02$  $24 \pm 1$  $0.38 \pm 0.02$ 30 1084  $0.056 \pm 0.02$  $47.5 \pm 1.5$  $0.45 \pm 0.02$ 11.5  $62 \pm 1$  $0.36 \pm 0.02$ 40 0.89 1700  $91 \pm 2$  $0.054 \pm 0.02$  $38.5 \pm 1.5$ 

**TABLE I.** Linear and nonlinear properties of the suspensions investigated in this article.

strains that relax very slowly [39,40,41]. To overcome this difficulty, we have implemented two different protocols that are schematically represented in Fig. 4. In both protocols, the material is first presheared at a constant shear rate  $\dot{\gamma}_0$  for a time interval  $t_0$ . The values of  $\dot{\gamma}_0$  and  $t_0$  do not matter significantly provided that the yield stress is exceeded and the suspension is fully fluidized and at steady state. In most of the experiments reported in this work, we use  $\dot{\gamma}_0 = 20 \text{ s}^{-1}$  and  $t_0 = 120 \text{ s}$ . This preshear step is intended to erase the previous mechanical history experienced by the suspension. At t = 0, the preshear flow is interrupted and the suspension is kept under zero shear stress in protocol A—see Fig. 4(A)—or under zero shear rate in protocol B—see Fig. 4(B)—during the waiting time  $t_w$ . Finally, at  $t = t_w$ , the probe shear rate  $\dot{\gamma}$  is applied and the stress is recorded until steady state is reached.

Figure 4(A') shows the strain recovery experienced by the microgel suspension when the stress is set to zero after the preshear is stopped (protocol A). At very short times  $(\Delta t < 200 \text{ ms})$ , the strain oscillates under the combined action of inertia and elasticity (data not shown). Then after a sharp drop, it slowly recovers in the direction opposite to the preshear. This demonstrates that the preshear flow has imprinted a directional strain into the microgel suspension,

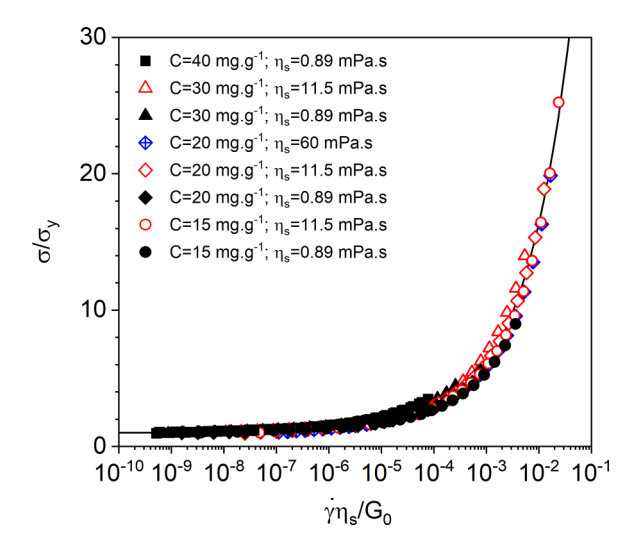


**FIG. 3.** Collapse of the experimental flow curves measured in the soft jamming regime onto a single master curve. The equation of the continuous line is  $\sigma/\sigma_y = 1 + 140(\dot{\gamma}\eta_S/G_0)^{0.48\pm0.02}$ . The original data are represented in Fig. S3 [48].

which forces the measuring geometry to rotate in the opposite direction. Similarly, Fig. 4(B') shows the stress relaxation experienced by the microgel suspension when it is immobilized after flow cessation (protocol B). The stress exhibits a fast initial decay followed by a much slower relaxation that persists over the longest times investigated [40,41]. These results show that although the preshear step prepares the suspensions in a reproducible rheological state, the subsequent startup flow experiments probe materials that are intrinsically out-of-equilibrium even after long waiting times. In the following, we analyze whether and to what extent residual stresses and strains affect the transient response of microgel glasses upon flow inception.

#### 2. Reversibility of the startup flow response

Preshear imparts a directional memory inside the suspension that remembers the last direction it has been sheared for

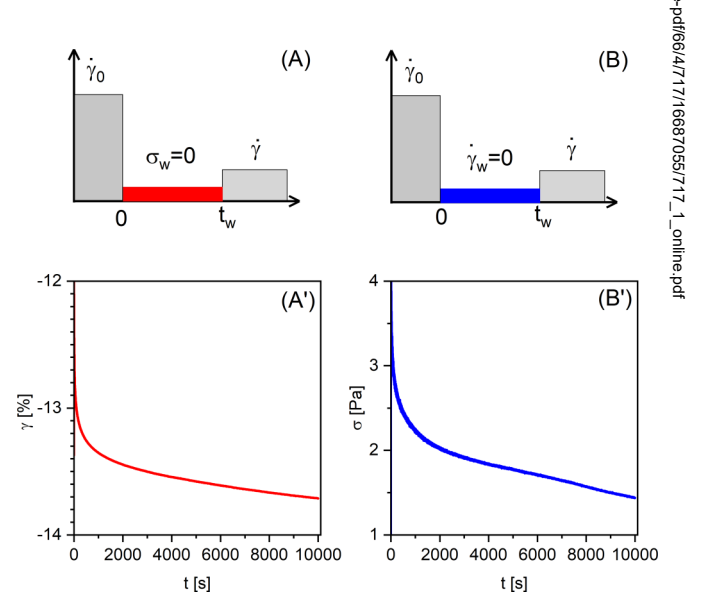


**FIG. 4.** Diagrams (A) and (B) represent the mechanical history for the two different experimental protocols used in this study. The material is first presheared by applying a constant shear rate  $\dot{\gamma}_0$  for a time interval  $t_0$ ; upon flow cessation, it is allowed to recover at zero shear rate (A) or relax at zero stress (B) for a period of time  $t_w$ ; then a shear rate of amplitude  $\dot{\gamma}$  is applied at  $t_w$ . (A') shows the recovery of the residual strain during the waiting time  $t_w$  when  $\sigma_w = 0$ ; at very short times, the strain oscillates under the combined action of inertia and elasticity; the strain origin is taken at the maximum of the first oscillation. (B') shows the relaxation of the residual stress during the waiting time  $t_w$  when  $\dot{\gamma}_w = 0$ . The concentration of the microgel suspension is  $C = 15 \text{ mg g}^{-1}$  and the suspending fluid is pure water.

ownloaded from http://pubs.aip.org/sor/jor/art

a long period of time [40,41]. This memory effect can make the transient behavior of the suspensions dependent on the preshearing direction [54,55]. Here, we use it as a way to track the influence of the preshear on subsequent startup flow experiments. We consider that the directional disturbance introduced by the preshear is negligible when the response is reversible upon flow reversal [55]. Figure 5 presents the results of two series of experiments performed with protocols A and B, respectively, for increasing values of  $t_w$ . For each value of  $t_w$ , we present the stress variations measured when (i) the preshear and the shear rate are applied along the same direction with  $\dot{\gamma}_0$ ,  $\dot{\gamma} > 0$  and (ii) they are applied along opposite directions with  $\dot{\gamma}_0 < 0$  and  $\dot{\gamma} > 0$ .

Let us first analyze the results shown in Figs. 5(A1)– 5(A4), which are obtained with protocol A, i.e., when  $\sigma_w = 0$ . The stress variations measured when the preshear and the applied shear rate are along the same direction  $(\dot{\gamma}_0, \ \dot{\gamma} > 0)$  qualitatively exhibit the characteristic shapes that are expected for startup flow experiments. The stress grows monotonically from a value close to zero, reaches a maximum which increases with the waiting time, and decreases to a steady-state value. When the preshear direction is reversed ( $\dot{\gamma}_0 < 0, \, \dot{\gamma} > 0$ ), the stress variations are affected, particularly at short waiting times, the stress overshoot being smaller and slightly shifted to lower strain values. However, above  $t_w = 1000 \,\mathrm{s}$ , the stress variations obtained for the preshear in the positive and negative directions are nearly superimposed, the stress maxima differing by less than 5% when  $t_w = 1000 \text{ s}.$ 

The results obtained with protocol B, i.e., when  $\dot{\gamma}_w = 0$ , are significantly different as shown in Figs. 5(B1)–5(B4).

First, the stress takes a finite value at low strain amplitude. This initial value is associated with the residual stress that has not relaxed during  $t_w$ ; it is positive or negative depending on the preshear direction. The presence of residual stress affects the entire response even for long waiting times. The stress overshoot is smaller and occurs later when the preshear is in the negative direction. Only at  $t_w = 10\,000\,\mathrm{s}$ , the response can be considered as reversible.

This study shows that protocol A minimizes the directional influence of the residual transient strains and stresses induced by the preshear on subsequent startup flow measurements. This conclusion is supported by the observation that, in protocol A, the residual stress measured at rest (applying  $\dot{\gamma} = 0$  g) for  $t > t_w$  is negligible once  $t_w$  is large enough, typically when  $t_w \ge 1000$  s, whereas in protocol B, a significant residual stress still exists and the response is not reversible upon reversal of the preshear direction—see Fig. S5 [48].

#### 3. Microscopic interpretation

In Fig. 6, we propose a microstructural interpretation of the origin of the memory effect and its consequence on startup flow experiments using the theoretical and experimental framework available from previous works [10,15,16,38,40,41]. In a fully equilibrated jammed glass at rest, soft particles are compressed with an equal number of neighbors in all directions: the pair distribution function is isotropic (see Fig. 6). Under a steady shear flow, the microstructure is distorted so that more particles are in the compressive region of the shear flow, where they are more compressed than at equilibrium, and fewer particles are in the extensional region where they are

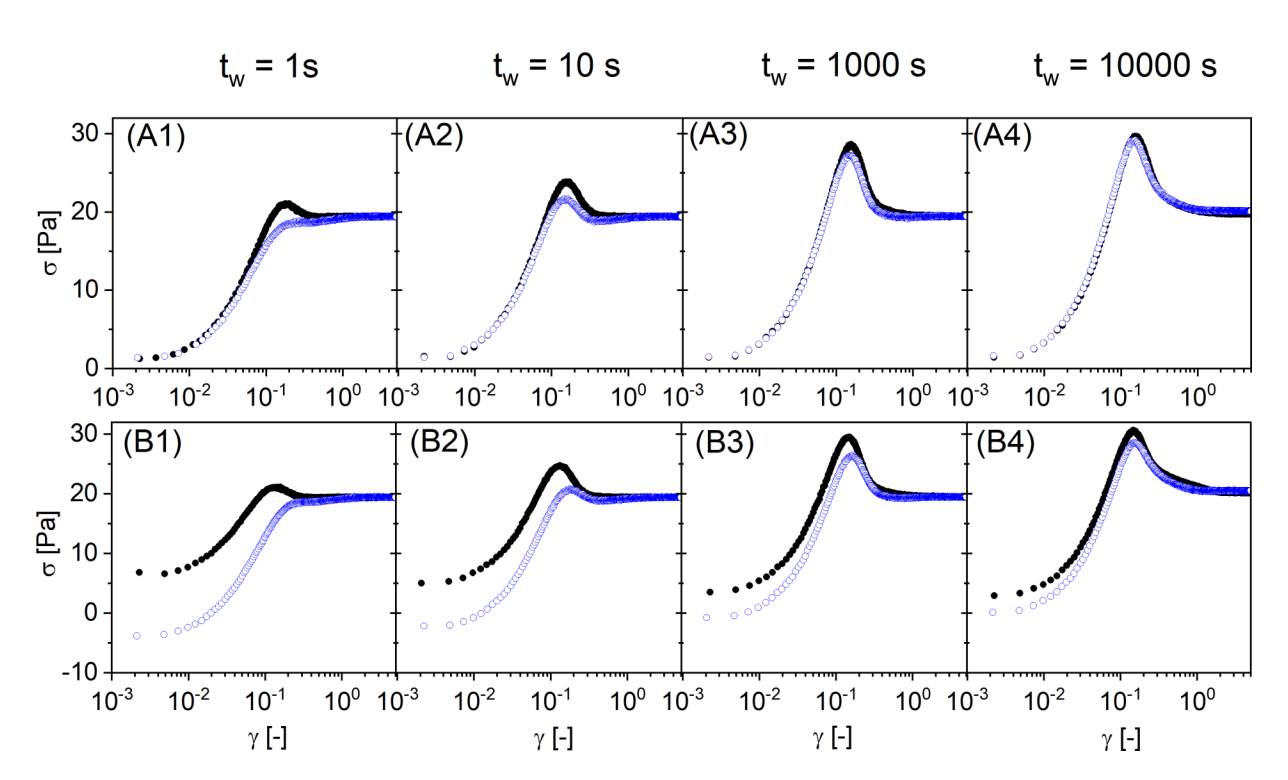


**FIG. 5.** Dependence of the stress response on the preshear direction for two protocols depicted in Figs. 4(A1)–4(A4):  $\sigma_w = 0$ ; Figs. 4(B1)–4(B4):  $\dot{\gamma}_w = 0$ . The shear rate  $\dot{\gamma} = 0.25 \text{ s}^{-1}$  is applied in the positive direction in all experiments, whereas the preshear is applied in the positive (black circles) or negative (blue open circles) direction. The origin of the strain is taken at the beginning of the startup flow experiments, i.e., at  $t = t_w$ . The concentration of the microgel suspension is  $C = 15 \text{ mg g}^{-1}$  and the suspending fluid is pure water ( $\eta_s = 0.89 \text{ mPa} \text{ s}$  at 20 °C). The amplitude of the preshear rate is  $|\dot{\gamma}_0| = 20 \text{ s}^{-1}$ .

마 e a c s: a re 사 d re

**FIG. 6.** Schematic representation of the two-dimensional pair distribution functions in the flow plane during preshear [(P) and (P')], at the beginning of startup flow experiments [(A), (A') and (B), (B')] and at steady state (S), following [40] and [41]. The dotted lines represent the pair distribution function when the glass is at rest and fully equilibrated. The arrows indicate the compression and extensional components of the flow relative to the test particle. During preshear, there appear an accumulation zone (continuous, black) and a depletion zone (dashed, black) in the compression and extension quadrants, respectively. In the compression quadrant, the particles are more compressed than in the quiescent state, whereas they are less compressed in the extension quadrant. There is no extra compression at  $t = t_w$  because the elastic recoil that relaxes compression and extension is a fast process. During the waiting time, the accumulation and depletion zones partly relax indicating the decay of anisotropy, which is coded by gray color and the length of the circular arcs. The preshear rate and the shear rate are applied during the startup flow, such as  $|\dot{\gamma}_0| > \dot{\gamma}$ .

less compressed as shown in Figs. 6(P) and 6(P') [10,35]. The resulting anisotropy of the pair distribution function is well characterized by the coefficient  $g_{2,-2}(r)$  of the expansion of the pair distribution function into an orthogonal series of spherical harmonics [56]. The macroscopic stress of soft particle glasses can then be directly computed from anisotropy through a simple expression, which involves the coefficient  $g_{2,-2}(r)$  and the amplitude of the elastic forces [10,17,38,40].

The variations of the shear stress growth function during the startup flow can be mapped onto the evolution of microstructural anisotropy. The situation where the suspension is initially fully equilibrated and the pair distribution function is isotropic has been investigated using simulations [38]. Upon flow inception, particles accumulate in the compressive direction beyond what is expected at a steady state. The stress overshoot represents the point where the anisotropy of the pair correlation function is maximum before being relaxed by rearrangements, which redistribute particle contacts. Upon flow cessation, the relaxation of the elastic deformation of particles, which only involves central elastic forces, is a fast process [41]. By contrast, the decay of anisotropy is slow because it requires collective rearrangements of large-scale configurations [39,41].

Let us now analyze the situation where a preshear flow is applied to the suspension prior to the startup flow experiment. When the preshear is stopped and zero stress is applied to the jammed suspension ( $\sigma_w = 0$ ; protocol A), the anisotropy created by the preshear persists for some time after flow cessation so that the stress in the suspension can be nonzero even though the macroscopic stress at the walls is zero. This residual stress forces the material to move in the direction opposite to the preshear. However, the anisotropy slowly relaxes so that the residual stress vanishes when the waiting time  $t_W$  is long enough, whatever the direction of the preshear, as illustrated in Figs. 6(A) and 6(A') (see also

supplementary material [48]) [46]. Therefore, at long waiting times, residual stresses do not affect subsequent startup flow experiments; the transient response is nearly reversible upon preshear reversal in agreement with the results shown in Figs. 5(A1)–5(A4).

When the jammed suspension is maintained at rest after preshearing ( $\dot{\gamma}_w = 0$ ; protocol B), a significant anisotropy whose orientation depends on the direction of the preshear persists for a long time after flow cessation [40,41], as illustrated in Figs. 6(B) and 6(B'). This anisotropy gives rise to a long-lived positive or negative residual stress. When the preshear is applied along the positive direction ( $\dot{\gamma}_0 > 0$ ), the residual anisotropy at the beginning of the startup flow in Fig. 6(B) has the same orientation as it will have at a steady state in Fig. 6(S). The buildup of the stress overshoot simply corresponds to a redistribution of compressed particles in the  $\frac{\sigma}{8}$ accumulation/depletion zones compatible with the applied shear rate  $\dot{\gamma} > 0$ . By contrast, when the preshear is applied in the negative direction ( $\dot{\gamma}_0 < 0$ ), the orientation of the anisotropy has to rotate by an angle  $\pi/2$  between the beginning of the startup flow experiment and the steady state [compare Figs. 6(B') and 6(S)]. It is likely that the anisotropy due to the preshear, which gives a negative contribution to the stress, coexists for some time with the anisotropy created by the applied shear rate  $\dot{\gamma}$ , which contributes positively to the stress. Therefore, the amplitude of the overshoot is smaller and its position shifted to higher strain with respect to the previous situation, just as observed in Figs. 5(B1)–5(B4).

#### B. Aging

In this section, we investigate the role of the waiting time  $t_w$  during which the suspension is allowed to recover  $(\sigma_w = 0)$  or to relax  $(\dot{\gamma}_w = 0)$  after the preshear step. Figure 7 presents two series of experiments performed using

Downloaded from http://pub

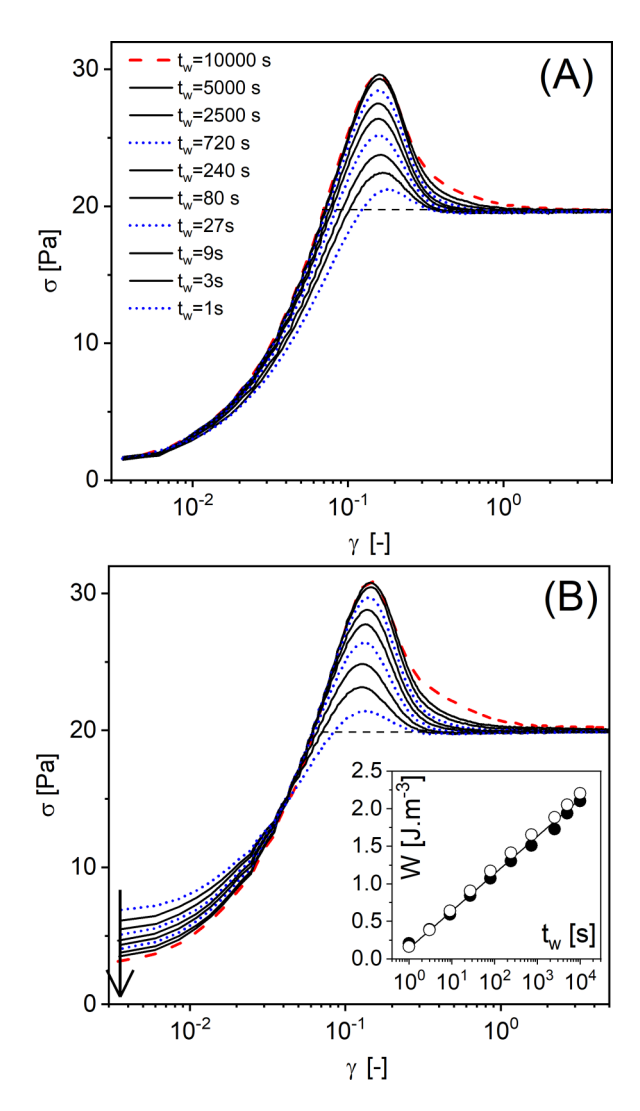


**FIG. 7.** Dependence of the stress response on the waiting time  $t_w$  for the two protocols is depicted in Fig. 4: (A)  $\sigma_w = 0$ ; (B)  $\dot{\gamma}_w = 0$ . The applied shear rate is  $\dot{\gamma} = 0.25 \text{ s}^{-1}$ . The suspension is presheared at a rate of  $\dot{\gamma}_0 = 20 \text{ s}^{-1}$  during 100 s. The origin of the strain is taken at the beginning of the startup flow experiment, i.e., at  $t = t_w$ . The concentration of the microgel suspension is  $C = 15 \text{ mg g}^{-1}$ ; the suspending fluid is pure water  $(\eta_s = 0.89 \text{ mPa s at } 20 \,^{\circ}\text{C})$ . The inset in panel (B) shows the variations of the work of yielding per unit volume defined as the peak area above the dashed lines, as a function of the waiting time.

the two protocols described in Sec. III A 1 when the waiting time is increased from 1 to  $10^4$  s. Both the preshear rate  $\dot{\gamma}_0$ and the shear rate  $\dot{\gamma}$  are applied along the positive direction. Figure 7(A) depicts the results obtained with protocol A, i.e., when  $\sigma_w = 0$ . The stress grows monotonically from a value close to zero, which confirms that the residual stress at  $t_w$  is very small, goes through a maximum, and decreases to a steady-state value. The amplitude of the stress overshoot  $(\sigma_p)$ , which is very small at short waiting times, increases significantly with  $t_w$  before saturating at very long times  $(t_w > 2500 \text{ s})$ . The peak then becomes broader. The position of the peak is nearly independent of the waiting time except at very short waiting times where there is some residual anisotropy. Figure 7(B) is obtained using protocol B  $(\dot{\gamma}_w = 0)$ . The time evolution of the peak overshoot follows the same trends as in protocol A except at small strain values (i.e., short times) where the response is affected by the presence of a significant residual stress as discussed in Sec. III A. This initial stress decreases as the waiting time is increased as expected. The startup flow curves measured for different waiting curves all cross over at a strain of about 0.04, which represents the strain above which the residual stress due to preshear becomes negligible compared to the stress induced by the applied shear rate as the initial anisotropy is progressively erased by local rearrangements.

It is interesting to discuss these findings in the context of the recent literature. The results depicted in Fig. 7 are in qualitative agreement with previous observations reported for various soft colloidal materials [20–24,30,34]. The increase in the amplitude of the stress overshoot is generally associated with aging phenomena. Our experimental results are also well reproduced by the particle dynamics simulation described in [38], which confirms that aging in jammed glasses is driven by the long time evolution of local particle configurations in the mechanical energy landscape. To be quantitative, we compute the mechanical work associated with yielding by integrating the area under the peak associated with the stress overshoot. This method takes into account both the increase in the peak intensity at short time and its broadening at long time. The graph in the inset of Fig. 7(B) shows that \( \frac{1}{2} \) the mechanical works per unit volume computed for protocols § A  $(\sigma_w = 0)$  and B  $(\dot{\gamma}_w = 0)$  are comparable and follow a logarithmic variation over the entire of waiting time investigated. Such logarithmic functions of the waiting times have been demonstrated theoretically to be generic signatures of physical aging in disordered systems [57].

It is remarkable that the mechanical work associated to yielding is very small when the waiting time is short, in 5 agreement with the fact that the peak overshoot nearly disappears. This suggests that unrelaxed residual stresses and \( \frac{\delta}{2} \) strain create enough mobility to facilitate rearrangements that prevent large accumulation of particles in the compression \$\overline{8}\$ direction [41]. There is a striking analogy here with the behavior of thermal molecular glass formers annealed at high temperatures and quenched at T = 0 [31]. For poor annealing conditions, i.e., when the initial amorphous state is prepared at high temperatures where the local environments fluctuate,  $\bar{\xi}$ yielding is monotonous without stress overshoots. When the glass formers are quenched deeper inside the glass phase, there are fewer fluctuations and a stress overshoot appears. In this analogy, soft glasses are mechanically activated and residual local stress plays the role of the temperature in glass formers, the annealing being controlled by the waiting time. Note however that there is a third regime in glass formers, where yielding becomes discontinuous with a sharp drop of the stress around a yield strain of about 0.12. Although this regime is not observed here, additional experiments would be useful to check that discontinuous yielding never occurs at much longer waiting times in SPGs.

#### C. Role of shear rate

We are now in a position to perform startup flow experiments where the applied shear rate is systematically varied from  $10^{-3}$  to  $4 \,\mathrm{s}^{-1}$ . In all these experiments, the suspensions are presheared by applying a constant shear rate of  $\dot{\gamma}_0 = 20 \, \mathrm{s}^{-1}$  for

100 s and the waiting time is  $t_w = 1000$  s above which the peak stresses do not evolve significantly. Figures 8(A) and 8(B) present the results obtained with protocol A ( $\sigma_w = 0$ ) and B  $(\dot{\gamma}_w = 0)$  when the concentration is  $C = 15 \text{ mg g}^{-1}$ . The variations of the stress overshoot with the applied shear rate in both sets of data exhibit the same trend: the overshoot is very small at low applied shear rates and increases with the applied shear rate. There is, however, one important difference when one considers the small strain limit of the stress: the initial stress in Fig. 8(A) is zero as expected, but in Fig. 8(B), it takes a constant value associated with the value of the unrelaxed residual stress at the beginning of the experiment. The long time values obtained at steady state are insensitive to the mechanical history as expected. The inset in Fig. 8(B) compares the values of the stress overshoot  $\sigma_p$  and of its position  $\gamma_p$  as a function of the applied shear rate, which are obtained in protocols A and B. The value of  $\sigma_p$  is slightly larger in protocol B than it is in A, indicating that the unrelaxed residual stress adds a small contribution to the static yield stress. By contrast, the suspensions yield earlier

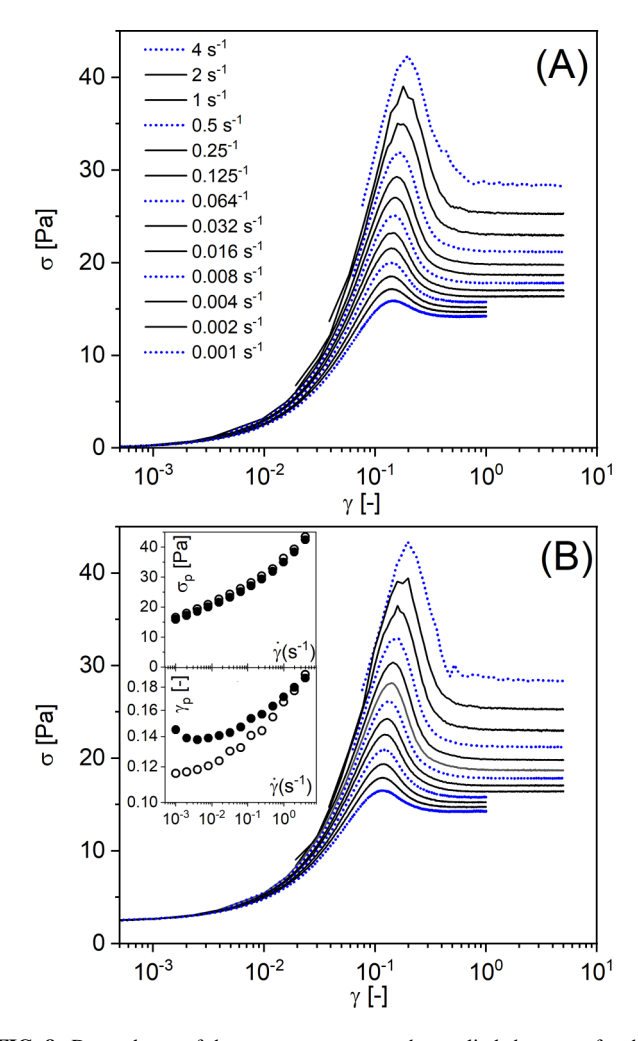


**FIG. 8.** Dependence of the stress response on the applied shear rate for the two protocols is depicted in Fig. 4: (A)  $\sigma_w = 0$ ; (B)  $\dot{\gamma}_w = 0$ . The origin of the strain is taken at the beginning of the startup flow experiments, i.e., at  $t = t_w$  ( $t_w = 1000$  s). The concentration of the microgel suspension is C = 15 mg g<sup>-1</sup>; the suspending liquid is pure water ( $\eta_s = 0.89$  mPa s at 20 °C). The inset in panel (B) compares the values of the static yield stress and static yield strain obtained with protocol A (black circles) and B (open circles).

in protocol B. This can be understood by considering that there is a pre-existing anisotropy in B, at the beginning of the experiment, which facilitates the yielding process. The yield strain in protocol A exhibits a small upturn at very low applied yield strain, which we attribute to some contribution of the unrelaxed strain when  $\sigma_w = 0$ . The same trends are found over a wide range of concentrations and for different viscosities of the suspending liquid, which are the two main parameters controlling the static yield stress and static yield strain.

The raw values are reported in Fig. 9 for different concentrations and solvent viscosities. We observe that  $\sigma_p$  at a given shear rate varies by a factor 10. The range of variation of  $\gamma_p$  is narrower. The values of  $\sigma_p$  and  $\gamma_p$  increase with the polymer concentration. At a given concentration, both quantities also increase with the solvent viscosity.

## D. Scaling properties of the static yield stress and static yield strain and comparison with simulations

Let us now rationalize the dependence of the static yield p stress and yield strain on microgel concentration and suspending fluid viscosity. In Figs. 10(A) and 10(B), following our previous work [36], we plot the variations of the dimensionless static yield stress  $\sigma_p/\sigma_v$  versus the reduced shear rate  $\dot{\gamma}\eta_S/G_0$ .  $\eta_s$  is the viscosity of the suspending fluid,  $G_0$  is the plateau modulus, and  $\sigma_v$  is the dynamic yield stress  $\bar{b}$ determined from flow curve measurements (see Table I). All the data collapse and form a unique master curve over several decades of shear rates. We do not observe any significant differences between the static yield stresses measured with protocols A and B, respectively. We have also  $\frac{\overline{\Phi}}{\overline{\Phi}}$ reported the values computed numerically using our 3D particle dynamics simulations for three different volume fractions. The theoretical and experimental data are in good agreement within the accuracy of the simulations and experiments. It is interesting to note that the variable  $\sigma_p/\sigma_v$  is  $\mathfrak{F}$ similar to the reduced stress  $\sigma/\sigma_v$  which is used to collapse  $\vec{\beta}$ the steady-state flow curves on universal master curves in 5 Fig. 3 [1,11,19,53]. This similarity arises from the fact that both the stress at steady state and the stress overshoot have the anisotropy of the pair distribution function as a common origin.

In Figs. 10(C) and 10(D), we plot the variations of the static yield strain determined with protocols A and B, respectively, as a function of the dimensionless shear rate  $\dot{\gamma}\eta_S/G_0$ . Again the data collapse on master curves, albeit with some dispersion. We note that, however, the data measured using protocol A ( $\sigma_W=0$ ) are systematically larger than the results obtained with protocol B ( $\dot{\gamma}_W=0$ ). In the former case, the yield strain data tend to the limit  $\gamma\cong0.15$  when  $\dot{\gamma}\to0$ , whereas in the latter they approach 0.1. The data obtained from simulations tend to  $\gamma\cong0.1$ , but they are slightly smaller than the experimental data that lay above.

#### IV. CONCLUDING REMARKS

Our results demonstrate that it is crucial to take into account the mechanical history to understand the transient yielding of SPGs. The conventional protocol widely used in

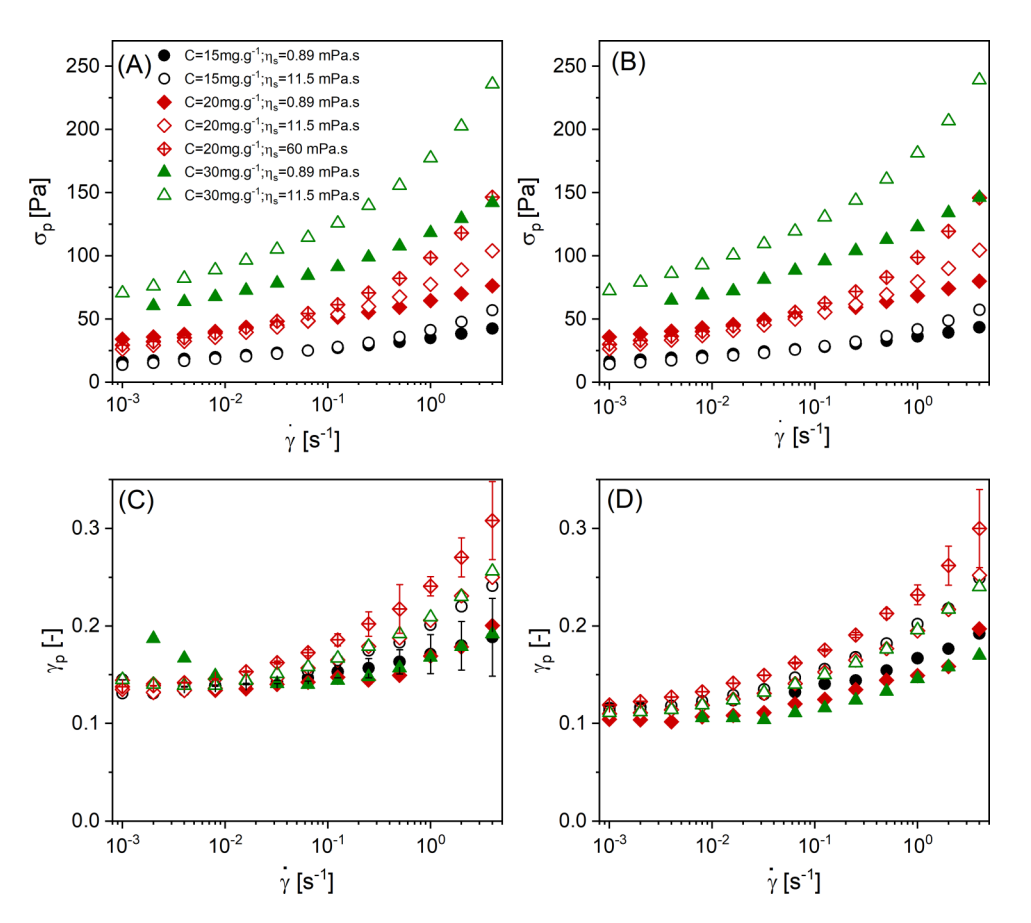


**FIG. 9.** Static yield stress  $\sigma_p$  and corresponding static yield strain  $\gamma_p$  as a function of the applied shear rate for the two protocols are depicted in Fig. 4: (A) and (C)  $\sigma_w = 0$ ; (B) and (D)  $\dot{\gamma}_w = 0$ . The concentration of the suspensions and the solvent viscosity are varied.

the literature, which consists in preshearing the material to put it in a reproducible state, creates long-lived internal stresses or strains that slowly recover and affect subsequent startup experiments in two ways. First, the material keeps a memory of the direction along which it has been presheared. The transient response is not reversible upon flow reversal and depends on the direction of the preshear relatively to the direction of the applied shear rate. Second, the stress response evolves with the time elapsed after the end of the preshear, the so-called waiting time: the peak overshoot grows in amplitude and becomes broader at long waiting times. The mechanical work associated with yielding increases with the waiting time in a logarithmic way, which is indicative of physical aging [57]. Here, physical aging is driven by the disordered distribution of internal stresses introduced during preshearing. Poorly annealed SPGs, i.e., when the waiting time is short, tend to yield in a continuous manner without stress overshoot because internal stresses create some local mobility that favor particle rearrangements [41].

We have designed and implemented the experimental protocol (A) that minimizes the directional memory and restore reversibility upon flow reversal. After preshearing, the material is allowed to recover by applying zero macroscopic stress for a long enough time. We anticipate that internal stresses' distribution is then symmetrical, which explains the absence of directional bias and restoring reversibility upon flow reversal. The dual protocol (B) that consists in annealing the material after preshear by applying zero shear rate requires much

longer annealing times and is not fully efficient for our purpose. In this second protocol, internal stresses persist long after flow cessation and affect the transient rheology of SPGs until they reach steady state. In this regard, our results open promising perspectives to prepare materials with controlled internal stress distributions.

The reduced static yield stress data  $\sigma_p/\sigma_y$ , where  $\sigma_y$  is the dynamic yield stress measured from steady flow measurements, collapse onto a universal master curve when they are plotted as a function of the dimensionless shear rate  $\dot{\gamma}\eta_S/G_0$ . The scope of this result is twofold. First, it confirms that the dynamic yield stress is the appropriate scale to rationalize the variations of the static yield stress. Second, it supports the importance of the dimensionless variable  $\dot{\gamma}\eta_S/G_0$  and of the characteristic time  $\eta_s/G_0$  to rationalize the transient rheology of SPGs in addition to the steady-state properties [1,11,18,19,38,53]. The static yield stresses obtained with the optimized protocol (A) and the protocol (B) that only provides partial stress annealing are comparable within a difference of about 10%. A common trend observed in both protocols is that the peak overshoot vanishes when the applied shear rate is small and increases rapidly when it is large. This can be understood by considering that the duration of rearrangements is set by the characteristic time  $\eta_s/G_0$  [19]. Therefore, when  $\dot{\gamma}\eta_{\rm S}/G_0\ll 1$ , local plastic rearrangements can occur before macroscopic yielding takes place. On the opposite limit where  $\dot{\gamma}\eta_{\rm S}/G_0\gg 1$ , particles are trapped in their cages and accumulate elastic energy until cages break, which happens in the

Downloaded from http://pubs.aip.org/

vicinity of the stress overshoot, thus confirming the connection we proposed earlier between the transient rheology of SPGs and the microscopic dynamics [38].

The experimental master curves obtained by plotting the reduced shear rate  $\sigma_p/\sigma_v$  as a function of the dimensionless shear rate  $\dot{\gamma}\eta_S/G_0$  are in good agreement with the similar master curve formed by the simulation data. This is an interesting outcome considering the relatively small size of the simulations. In the simulations, we have shown that the structural anisotropy revealed by the pair distribution function g(r) controls the stress buildup, the latter reaching a maximum at the stress overshoot before being relaxed by particle rearrangements. It is interesting to note that the variations of the reduced static yield stress versus the nondimensional shear rate in Figs. 10(A) and 10(B) exhibit some similarity with the master flow curve as shown in Fig. 3. We believe that this similarity expresses that the stress overshoot and the stress at steady state are controlled by the same physical mechanism, i.e., the anisotropy of the pair distribution function.

The static yield strain values  $\gamma_p$  measured for different materials collapse reasonably well onto master curves for both protocols A and B. However, the quality of the collapse is affected by some dispersion in the data. The master curves are found to be slightly dependent on the measuring protocol and they are shifted with respect to the master curve obtained

in simulations, the discrepancy being the greater for the data measured using protocol A.

In order to assess the generality of the results presented in this article, we have investigated the startup flow properties of two additional soft particle glasses. The first system is made of microgels that have the same composition as in this study except for the nature of the crosslinker, which is dicyclopentenyl-oxyethyl methacrylate [3]. The degrees of crosslinking are comparable as well as the particle size. These microgels are also synthesized using emulsion polymerization, but there are some differences in the temperature of the reaction and the rate of addition of the reactants. The crosslinker is more hydrophobic than diallyl phthalate, which is used in this study, which can induce some variability in the spatial distribution of the crosslinker inside the microgels. We restrict our discussion to the values of the reduced static yield stress  $\sigma_p/\sigma_v$  and yield strain  $\gamma_p$  obtained using protocol A ( $\sigma_w = 0$ ), which are presented in supplementary material [48]. The values of  $\sigma_p/\sigma_v$  obtained for different concentrations and solvent viscosities collapse very well on a unique master curve in very good agreement with the simulations, when they are plotted as a function of the dimensionless shear rate  $\dot{\gamma}\eta_{\rm S}/G_0$ . We just note the absence of static yield  $\underline{\underline{\beta}}$ stress below a dimensionless shear rate of about  $10^{-7}$ , whereas in Fig. 10(A), there is still a small stress overshoot at a dimensionless shear rate of about  $10^{-9}$ . An important .aip.org/sor/jor/article-pdf/66/4/717/16687055/717\_1\_online.pdf

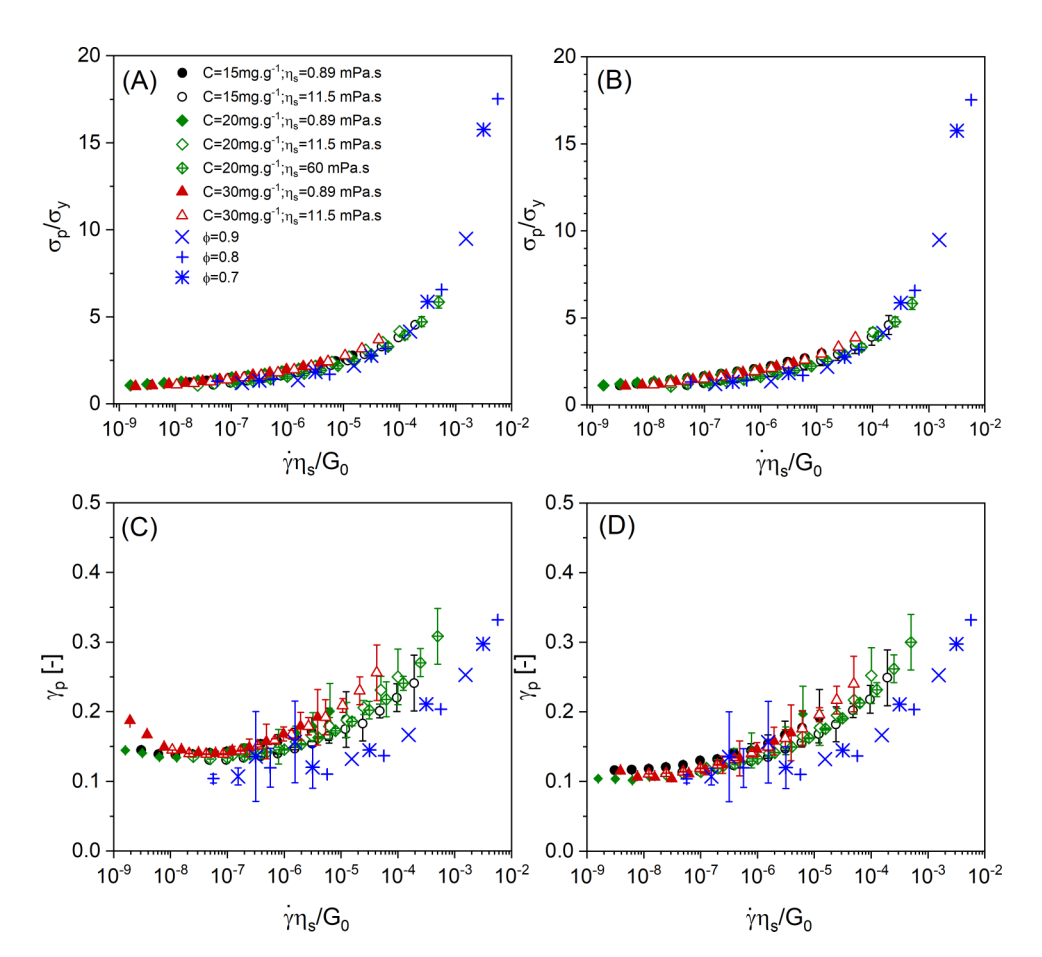


**FIG. 10.** Reduced static yield stress  $\sigma_p/\sigma_y$  (A) and (B) and corresponding static yield strain  $\gamma_p$  (C) and (D) as a function of the reduced shear rate for microgel suspensions with varying concentrations and solvent viscosities using the two protocols depicted in Fig. 4: (A) and (C)  $\sigma_w = 0$ ; (B) and (D)  $\dot{\gamma}_w = 0$  The blue crosses represent the simulation data replotted from [38]. The coding of the data (symbols and colors) is the same as in Fig. 9.

difference between the two systems concerns the static yield strain variations. The values of  $\gamma_p$  are of the same order of magnitude as in Fig. 10(C), but they do not collapse on a single master curve. This suggests that the position of the stress overshoot in startup flow experiments is influenced by details of the microstructure and contact interactions. The second system is made of Carbopol particles at different concentrations as studied in [32] (see supplementary material [48]). The preparation protocol and the aging time are not specified in the original publication, which may introduce a bias in comparison with our experiments. When plotted as a function of the dimensional shear rate  $\dot{\gamma}\eta_S/G_0$ , the reduced shear stress data  $\sigma_p/\sigma_v$  collapse on a curve, which is shifted vertically with respect to the master curve found for the microgels and the simulations. The stress overshoots occur for strain values much larger than reported in this study. Again the static yield strain data  $\gamma_p$  do not collapse. To conclude this discussion, although the scaling properties of the static yield stress found for different SPGs in experiments and simulations agree altogether, the behavior of the static yield strain is far less universal. We attribute the observed differences in part to experimental errors and to the sensitivity of the static yield strain to the exact microstructure of the particles.

The behavior described in this study exhibits interesting similarities with that of hard sphere suspensions. Flow cessation in hard sphere suspensions is followed by slow relaxation or recovery, when the shear rate or the stress is set to zero, respectively, until an arrested state is reached [58]. Moreover, the growth of the stress during the startup flow is associated with microstructural anisotropy [35,36]. There is, however, an important difference between hard sphere glasses where the stress overshoot decreases when the volume fraction approaches random close-packing, i.e., the jamming transition of hard spheres and soft colloids where the stress overshoot increases in a monotonic way with the volume fraction. This can be qualitatively justified by the fundamental difference that exists between hard and soft sphere suspensions. In hardsphere glasses, the stress is of entropic origin, the free volume decreases drastically near close-packing so that no large deformation nor stress accumulation is possible. This restriction does not exist in soft particle glasses where particles are in contact and have the capacity to deform both in compressive and in extension directions causing an increase in structural anisotropy and accumulation of elastic energy.

Although the buildup of anisotropy in relation to the accumulation/depletion mechanism appears to be a generic mechanism in particulate materials, albeit with some subtle variations, its relevance for other soft matter systems like polymers is an open question. The startup behavior of entangled linear chains in melts has been extensively studied (see [59] and references therein). It depends on the relative value of the applied shear rate and the frequencies associated with terminal relaxation  $(\omega_d)$  and Rouse relaxation  $(\omega_R)$ . When  $\dot{\gamma} < \omega_d$ , the stress grows monotonically toward the steady state value without any overshoot. At larger shear rates,  $\omega_d < \dot{\gamma} < \omega_R$ , there is an overshoot at  $\gamma_p \cong 2.3$ , which is much larger than in soft particle glasses. The overshoot is explained by the orientation of the chain segments in their tube. At still larger shear rates,  $\dot{\gamma} > \omega_R$ , the chains do not have time to equilibrate in their tube and the overshoot involves a combination of segment orientation and chain stretching. The situation is still more complex in entangled branched polymers where the stress growth is characterized by a double overshoot due to a combination of orientation, stretching, and lateral branch dynamics [60]. Polymer glasses also exhibit a rich phenomenology with the stress overshoot depending on temperature, applied shear rate, and mechanical history [61]. In these systems, plastic deformation is homogeneous at scales larger than the entanglement lengths, but distortions occur at smaller scales comparable to the monomer size [62]. In conclusion, irrespective of the system under investigation, start-up flow experiments appear to be critical and challenging tools that are sensitive to topology and reflect the microscopic dynamics.

#### **ACKNOWLEDGMENTS**

B.F.D.D. and M.C. acknowledge financial support from the Innovative Training Network Dodynet (European No. 765811). They are indebted to Jean-Marc Suau (Coatex \( \frac{5}{6} \) SAS) who provided the microgels used in this study. They also thank Andre Braun and Jörg Laeuger from Anton Paar টু for their technical help in the optimization of the transient measurements. F.K. and R.T.B. gratefully acknowledge financial support from the National Science Foundation financial support from the National Science Foundation (NSF) (MRSEC under Award No. DMR-1720595).

AUTHOR DECLARATIONS

Conflict of Interest

The authors have no conflicts to disclose.

REFERENCES

[1] Bonnecaze, R. T., and M. Cloitre, Micromechanics of soft particle of glasses, in High Solid Dispersions, edited by M. Cloitre (Springer) (NSF) (MRSEC under Award No. DMR-1720595).

#### **AUTHOR DECLARATIONS**

#### **Conflict of Interest**

#### REFERENCES

- glasses, in High Solid Dispersions, edited by M. Cloitre (Springer Berlin, Heidelberg, 2010), pp. 117-161.
- [2] Vlassopoulos, D., and M. Cloitre, "Tunable rheology of dense soft deformable colloids," Curr. Opin. Colloid Interface Sci. 19(6), 561-574 (2014).
- [3] Pellet, C., and M. Cloitre, "The glass and jamming transitions of soft polyelectrolyte microgel suspensions," Soft Matter 12(16), 3710-3720 (2016).
- [4] Erwin, B. M., M. Cloitre, M. Gauthier, and D. Vlassopoulos, "Dynamics and rheology of colloidal star polymers," Soft Matter 6(12), 2825-2833 (2010).
- [5] Gury, L., M. Gauthier, M. Cloitre, and D. Vlassopoulos, "Colloidal jamming in multiarm star polymer melts," Macromolecules 52(12), 4617-4623 (2019).
- [6] Parisi, D., E. Buenning, N. Kalafatakis, L. Gury, B. C. Benicewicz, M. Gauthier, M. Cloitre, M. Rubinstein, S. K. Kumar, and D. Vlassopoulos, "Universal polymeric-to-colloidal transition in melts of hairy nanoparticles," ACS Nano 15(10), 16697-16708 (2021).
- [7] Bonn, D., M. M. Denn, L. Berthier, T. Divoux, and S. Manneville, "Yield stress materials in soft condensed matter," Rev. Mod. Phys. 89(3), 035005 (2017).
- [8] Vlassopoulos, D., and M. Cloitre, Soft colloids, in Theory and Applications of Colloidal Suspension Rheology (Cambridge University, Cambridge, 2021).

- [9] Siebenbürger, M., M. Fuchs, H. Winter, and M. Ballauff, "Viscoelasticity and shear flow of concentrated, noncrystallizing colloidal suspensions: Comparison with mode-coupling theory," J. Rheol. 53(3), 707–726 (2009).
- [10] Seth, J. R., L. Mohan, C. Locatelli-Champagne, M. Cloitre, and R. T. Bonnecaze, "A micromechanical model to predict the flow of soft particle glasses," Nat. Mater. 10(11), 838–843 (2011).
- [11] Liu, T., F. Khabaz, R. T. Bonnecaze, and M. Cloitre, "On the universality of the flow properties of soft-particle glasses," Soft Matter 14(34), 7064–7074 (2018).
- [12] Sollich, P., "Rheological constitutive equation for a model of soft glassy materials," Phys. Rev. E 58(1), 738–759 (1998).
- [13] Nicolas, A., E. E. Ferrero, K. Martens, and J.-L. Barrat, "Deformation and flow of amorphous solids: Insights from elastoplastic models," Rev. Mod. Phys. 90(4), 045006 (2018).
- [14] Kamani, K., G. J. Donley, and S. A. Rogers, "Unification of the rheological physics of yield stress fluids," Phys. Rev. Lett. 126(21), 218002 (2021).
- [15] Cuny, N., R. Mari, and E. Bertin, "Microscopic theory for the rheology of jammed soft suspensions," Phys. Rev. Lett. 127(21), 218003 (2021).
- [16] Cuny, N., E. Bertin, and R. Mari, "Dynamics of microstructure anisotropy and rheology of soft jammed suspensions," Soft Matter 18(2), 328–339 (2022).
- [17] Mohan, L., C. Pellet, M. Cloitre, and R. Bonnecaze, "Local mobility and microstructure in periodically sheared soft particle glasses and their connection to macroscopic rheology," J. Rheol. 57(3), 1023–1046 (2013).
- [18] Khabaz, F., M. Cloitre, and R. T. Bonnecaze, "Structural state diagram of concentrated suspensions of jammed soft particles in oscillatory shear flow," Phys. Rev. Fluids 3(3), 033301 (2018).
- [19] Khabaz, F., M. Cloitre, and R. T. Bonnecaze, "Particle dynamics predicts shear rheology of soft particle glasses," J. Rheol. 64(2), 459–468 (2020).
- [20] Carrier, V., and G. Petekidis, "Nonlinear rheology of colloidal glasses of soft thermosensitive microgel particles," J. Rheol. 53(2), 245–273 (2009).
- [21] Koumakis, N., A. Pamvouxoglou, A. S. Poulos, and G. Petekidis, "Direct comparison of the rheology of model hard and soft particle glasses," Soft Matter 8(15), 4271–4284 (2012).
- [22] Derec, C., G. Ducouret, A. Ajdari, and F. Lequeux, "Aging and nonlinear rheology in suspensions of polyethylene oxide-protected silica particles," Phys. Rev. E 67(6), 061403 (2003).
- [23] Rogers, S. A., D. Vlassopoulos, and P. Callaghan, "Aging, yielding, and shear banding in soft colloidal glasses," Phys. Rev. Lett. 100(12), 128304 (2008).
- [24] Rogers, S. A., P. T. Callaghan, G. Petekidis, and D. Vlassopoulos, "Time-dependent rheology of colloidal star glasses," J. Rheol. 54(1), 133–158 (2010).
- [25] Partal, P., A. Guerrero, M. Berjano, and C. S. Gallegos, "Transient flow of O/W sucrose palmitate emulsions," J. Food Eng. 41(1), 33–41 (1999).
- [26] Ovarlez, G., S. Rodts, A. Ragouilliaux, P. Coussot, J. Goyon, and A. Colin, "Wide-gap Couette flows of dense emulsions: Local concentration measurements, and comparison between macroscopic and local constitutive law measurements through magnetic resonance imaging," Phys. Rev. E 78(3), 036307 (2008).
- [27] Dimitriou, C. J., and G. H. McKinley, "A comprehensive constitutive law for waxy crude oil: A thixotropic yield stress fluid," Soft Matter 10(35), 6619–6644 (2014).
- [28] Fernandes, R. B., D. E. V. Andrade, A. T. Franco, and C. O. R. Negrão, "The yielding and the linear-to-nonlinear viscoelastic

- transition of an elastoviscoplastic material," J. Rheol. **61**(5), 893–903 (2017)
- [29] Divoux, T., C. Barentin, and S. Manneville, "Stress overshoot in a simple yield stress fluid: An extensive study combining rheology and velocimetry," Soft Matter 7(19), 9335–9349 (2011).
- [30] Kurokawa, A., M. Ichihara, and K. Kurita, "Softening of aged fluids in start-up flows of dense suspensions," J. Non-Newtonian Fluid Mech. 217, 14–22 (2015).
- [31] Ozawa, M., L. Berthier, G. Biroli, A. Rosso, and G. Tarjus, "Random critical point separates brittle and ductile yielding transitions in amorphous materials," Proc. Natl. Acad. Sci. U.S.A. 115, 6656–6661 (2018)
- [32] Benzi, R., T. Divoux, C. Barentin, S. Manneville, M. Sbragaglia, and F. Toschi, "Stress overshoots in simple yield stress fluids," Phys. Rev. Lett. 127(14), 148003 (2021).
- [33] Jiang, M., G. Wilde, and L. Dai, "Origin of stress overshoot in amorphous solids," Mech. Mater. **81**, 72–83 (2015).
- [34] Amann, C. P., M. Siebenbürger, M. Krüger, F. Weysser, M. Ballauff, and M. Fuchs, "Overshoots in stress-strain curves: Colloid experiments and schematic mode coupling theory," J. Rheol. 57(1), 149–175 (2013).
- [35] Koumakis, N., M. Laurati, S. Egelhaaf, J. Brady, and G. Petekidis, "Yielding of hard-sphere glasses during start-up shear," Phys. Rev. Lett. 108(9), 098303 (2012).
- [36] Koumakis, N., M. Laurati, A. R. Jacob, K. J. Mutch, A. Abdellali, S. A. B. Schofield, S. U. Egelhaaf, J. F. Brady, and G. Petekidis, "Start-up shear of concentrated colloidal hard spheres: Stresses, dynamics, and structure," J. Rheol. **60**(4), 603–623 (2016).
- [37] Zaccone, A., P. Schall, and E. M. Terentjev, "Microscopic origin of gononlinear nonaffine deformation in bulk metallic glasses," Phys. Rev. **B** 90(14), 140203(R) (2014).
- [38] Khabaz, F., B. F. Di Dio, M. Cloitre, and R. T. Bonnecaze, "Transient dynamics of soft particle glasses in startup shear flow. Part I: Microstructure and time scales," J. Rheol. **65**(2), 241–255 (2021).
- [39] Cloitre, M., R. Borrega, and L. Leibler, "Rheological aging and rejuvenation in microgel pastes," Phys. Rev. Lett. **85**(22), 4819–4822 (2000).
- [40] Mohan, L., R. T. Bonnecaze, and M. Cloitre, "Microscopic origin of internal stresses in jammed soft particle suspensions," Phys. Rev. Lett. **911**(26), 268301 (2013).
- [41] Mohan, L., M. Cloitre, and R. T. Bonnecaze, "Build-up and two-steping relaxation of internal stress in jammed suspensions," J. Rheol. **59**(1), 63–84 (2015).
- [42] Goujard, S., Surfactant-activated microgels: Structure and dynamics, Ph.D. thesis, Paris Sciences et Lettres, 2019.
- [43] Cloitre, M., R. Borrega, F. Monti, and L. Leibler, "Structure and flow of polyelectrolyte microgels: From suspensions to glasses," C. R. Phys. 4, 221–230 (2003).
- [44] Borrega, R., M. Cloitre, I. Betremieux, B. Ernst, and L. Leibler, "Concentration dependence of the low-shear viscosity of polyelectrolyte micro-networks: From hard spheres to soft microgels," Europhys. Lett. 47(6), 729–735 (1999).
- [45] Romeo, G., L. Imperiali, J.-W. Kim, A. Fernàndez-Nieves, and D. A. Weitz, "Origin of de-swelling and dynamics of dense ionic microgel suspensions," J. Chem. Phys. 136(12), 124905 (2012).
- [46] Ghosh, A., G. Chaudhary, J. G. Kang, P. V. Braun, R. H. Ewoldt, and K. S. Schweizer, "Linear and nonlinear rheology and structural relaxation in dense glassy and jammed soft repulsive pNIPAM microgel suspensions," Soft Matter 15(5), 1038–1052 (2019).
- [47] Seth, J. R., M. Cloitre, and R. T. Bonnecaze, "Influence of short-range forces on wall-slip in microgel pastes," "J. Rheol. 52(5), 1241–1268 (2008).

Downloaded from I

.aip.org/sor/jor/article-pdf/66/4/717/16687055/717\_1

[48] See supplementary material at <a href="https://www.scitation.org/doi/suppl/10.1122/8.0000448">https://www.scitation.org/doi/suppl/10.1122/8.0000448</a> for transient response of rheometer, linear viscoelastic properties of microgel jammed glasses, steady flow properties of microgel jammed glasses, memory after strain recovery and stress relaxation, variations of the static yield stress and yield strain for microgels crosslinked with dicyclopentenyl-oxyethyl methacrylate, and variations of the static yield stress and yield strain for carbopol suspensions.

- [49] Mason, T. G., and D. A. Weitz, "Linear viscoelasticity of colloidal hard sphere suspensions near the glass transition," Phys. Rev. Lett. 75(14), 2770–2773 (1995).
- [50] Scheffold, F., F. Cardinaux, and T. G. Mason, "Linear and nonlinear rheology of dense emulsions: Identifying the glass and jamming regimes," J. Phys.: Condens. Matter 25, 502101 (2013).
- [51] Seth, J. R., M. Cloitre, and R. T. Bonnecaze, "Elastic properties of soft particle pastes," J. Rheol. 50(3), 353–376 (2006).
- [52] Ghosh, A., and K. S. Schweizer, "The role of collective elasticity on activated structural relaxation, yielding, and steady state flow in hard sphere fluids and colloidal suspensions under strong deformation," J. Chem. Phys. 153(19), 194502 (2020).
- [53] Cloitre, M., R. Borrega, F. Monti, and L. Leibler, "Glassy dynamics and flow properties of soft colloidal pastes," Phys. Rev. Lett. 90(6), 068303 (2003).
- [54] Letwimolnun, W., B. Vergnes, G. Ausias, and P. J. Carreau, "Stress overshoots of organoclay nanocomposites in transient shear flow," J. Non-Newtonian Fluid Mech. 141(2–3), 167–179 (2007).

- [55] Choi, J., and S. A. Rogers, "Optimal conditions for pre-shearing thixotropic or aging soft materials," Rheol. Acta 59, 921–934 (2020).
- [56] Hanley, H. J. M., J. C. Rainwater, and S. Hess, "Shear-induced dependence of the liquid pair correlation function," Phys. Rev. A 36(4), 1795–1802 (1987).
- [57 Lomholt, M] A., L. Lizana, R. Metzler, and T. Ambjörnsson, "Microscopic origin of the logarithmic time evolution of aging processes in complex systems," Phys. Rev. Lett. 110(20), 208301 (2013).
- [58] Pamvouxoglou, A., A. B. Schofield, G. Petekidis, and S. U. Egelhaaf, "Stress versus strain controlled shear: Yielding and relaxation of concentrated colloidal suspensions," J. Rheol. 65(6), 1219–1233 (2021).
- [59] Cao, J., and A. E. Likhtman, "Simulating startup shear of entangled polymer melts," ACS Macro Lett. 4(12), 1376–1381 (2015).
- [60] Snijkers, F., D. Vlassopoulos, G. Ianniruberto, G. Marrucci, H. Lee, J. Yang, and T. Chang, "Double stress overshoot in start-up of simple shear flow of entangled comb polymers," ACS Macro Lett. 2(7), 601–604 (2013).
- [61] Arruda, E. M., M. C. Boyce, and R. Jayachandran, "Effects of strain rate, temperature and thermomechanical coupling on the finite strain deformation of glassy polymers," Mech. Mater. 19(2-3), 193–212 (1995).
- [62] Casas, F., C. Alba-Simionesco, H. Montes, and F. Lequeux, Surface and Study, "Macromolecules 41(3), 860–865 (2008).

ed from http://pubs.aip.org/sor/jor/article-pdf/66/4/717/16687055/717\_1\_online.pdf